Czech Technical University
in Prague

Faculty of Nuclear Sciences and Physical
Engineering

Department of Physics

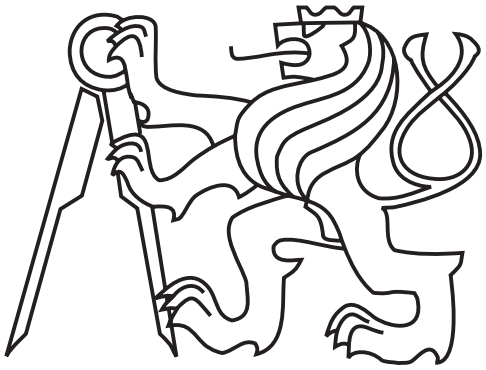

BACHELOR THESIS

Systematic calculations of hypernuclear spectra

Jan Pokorný

2016

Supervisor: Mgr. Petr Veselý, Ph.D.

Thesis title: **Systematic calculations of hypernuclear spectra**
Author: Jan Pokorný

Department: Department of Physics FNSPE CTU in Prague
Branch of study: Nuclear Engineering
Kind of thesis: Bachelor's Degree Project

Supervisor: Mgr. Petr Veselý, Ph.D.

Abstract: This thesis presents results of calculations of Λ single-particle spectra in ${}^{17}_{\Lambda}$O, ${}^{41}_{\Lambda}$Ca, and ${}^{209}_{\Lambda}$Pb, using a mean-field approach. The mean field is constructed self-consistently from the realistic NN interaction $\mathrm{N^2LO_{opt}}$ using the Hartree-Fock method. The Λ hyperon bound in a hypernucleus interacts with the nuclear medium through the effective YNG ΛN interaction derived from the Nijmegen model ESC08. The density-dependent DDNN interaction term which mimics three-body NNN forces was found to be essential for the correct description of nuclear and hypernuclear characteristics. The convergence and stability of the Λ single-particle spectra in ${}^{17}_{\Lambda}$O and ${}^{41}_{\Lambda}$Ca were studied as well, it was found that our results were in a good agreement with experimental data. We performed calculations using other NN and ΛN potentials and confirmed model independence of our predictions. We explored the dependence of the Λ single-particle spectrum in ${}^{41}_{\Lambda}$Ca on the coupling constant C_ρ and the Fermi momentum k_F entering the DDNN term and the YNG potential, respectively. We concluded that the correct values of C_ρ and k_F are needed in order to achieve reasonable description of Λ single-particle spectra.

Keywords: Λ hyperon, Λ hypernucleus, mean field, Hartree-Fock method

Název práce: **Systematické výpočty hyperjaderných spekter**
Autor: Jan Pokorný

Katedra: Katedra Fyziky FJFI ČVUT v Praze
Obor studia: Jaderné inženýrství
Druh práce: Bakalářská práce

Školitel: Mgr. Petr Veselý, Ph.D.

Abstrakt: Tato práce uvádí výsledky výpočtů jednočásticových spekter Λ hyperonu v ${}^{17}_{\Lambda}$O, ${}^{41}_{\Lambda}$Ca a ${}^{209}_{\Lambda}$Pb v přiblížení modelu středního pole. Střední pole je vytvořeno self-konzistentně z realistické NN interakce $\mathrm{N^2LO_{opt}}$ pomocí Hartree-Fockovy metody. Hyperon Λ vázaný v hyperjádře interaguje s jaderným prostředím skrze efektivní YNG ΛN interakci odvozenou z Nijmegenského modelu ESC08. Hustotně závislý DDNN interakční člen, který napodobuje roli tříčásticových NNN sil byl shledán nezbytným pro správný popis jaderných a hyperjaderných vlastností. Rovněž jsme studovali konvergenci a stabilitu jednočásticových spekter Λ v ${}^{17}_{\Lambda}$O a ${}^{41}_{\Lambda}$Ca a zjistili jsme, že naše výsledky jsou v souladu s experimentálními daty. Provedli jsme výpočty i s jinými NN a ΛN potenciály a potvrdili jsme modelovou nezávislost našich předpovědí. Zkoumali jsme závislost jednočásticového spektra Λ v ${}^{41}_{\Lambda}$Ca na vazbové konstantě C_ρ a Fermiho hybnosti k_F, které vstupují popořadě jako parametry do hustotně závislého DDNN interakčního členu a YNG potenciálu. Dospěli jsme k závěru, že správné hodnoty C_ρ a k_F jsou klíčové k rozumnému popisu jednočásticových spekter Λ.

Klíčová slova: hyperon Λ, Λ hyperjádro, střední pole, Hartree-Fockova metoda

Prohlášení

Prohlašuji, že jsem svou bakalářskou práci vypracoval samostatně a použil jsem pouze literaturu a publikace uvedené v přiloženém seznamu.

Souhlasím s použitím tohoto školního díla ve smyslu §60 Zákona č.121/1200Sb., o autorském právu, o právech souvisejících s autorským právem a o změně některých zákonů (autorský zákon).

Declaration

I declare that I wrote my bachelor thesis independently and exclusively within the use of cited bibliography.

I agree with the usage of this thesis in the purport of the Act 121/2000 (Copyright Act).

V Praze dne .....

.....

Acknowledgement

I would like to thank my supervisor Mgr. Petr Veselý, Ph.D. for his patience and professional guidance during writing this thesis. I would also like to thank RNDr. Jiří Mareš, CSc., Ing. Jaroslava Hrtánková, and Ing. Martin Schäfer for reading the manuscript and their invaluable objective criticism and help.

Contents

Chapter 1

Introduction

Hypernucleus is a bound system which consists of protons, neutrons and one or more hyperons (e.g. Λ, Σ, Ξ, Ω) with strangeness S $\neq 0$. Hyperons decay predominantly weakly (except Σ^0) which results in their rather long lifetime ($\approx 10^{-10}$ s) compared to the time scale of the strong interaction ($\approx 10^{-23}$ s). This allows experimental study of the properties of hypernuclei, including their structure. Furthermore, propagation of a hyperon in nuclear matter is not affected by the Pauli exclusion principle, which makes the hyperon a unique probe of the nuclear interior. The study of hypernuclei contributes to our better understanding of baryon-baryon forces, as well as nuclear structure and dynamics.

Hypernuclei were discovered in 1952 by Jerzy Pniewski and Maryan Danysz who explored interactions of high-energy cosmic ray with a nucleus in nuclear emulsion [1]. One of the events resulted in a heavy object that travelled a long distance before it decayed. This event is depicted in Fig. 1.1. First explanation was that this unknown object had been a bound system of a nucleus and π meson. However, this capture is highly improbable. Later, Pniewski and Danysz correctly concluded that the studied object was a bound system of nucleus and a hyperon [1]. In the late 1950's large number of hypernuclei has been discovered. Numerous species have been observed in experiments with nuclear emulsion exposed to proton, pion, or kaon beams. The data from these experiments were rather limited. Major breakthrough in hypernuclear physics has occurred due to the advent of counter experiments. The number of observed hypernuclei has been doubled and the information about their spectra has become more precise. Hypernuclei have been studied by many collaborations worldwide (CERN, BNL, KEK, FINUDA, JLab, JPARC, GSI, MAMI-C [2, 3, 4, 5, 6]). Their theoretical and experimental study is still topical.

Up to now, about 30 species of Λ hypernuclei have been discovered, starting from the lightest hypernuclear system ${}^{3}_{\Lambda}$H to the heaviest hypernuclei ${}^{208}_{\Lambda}$Pb and

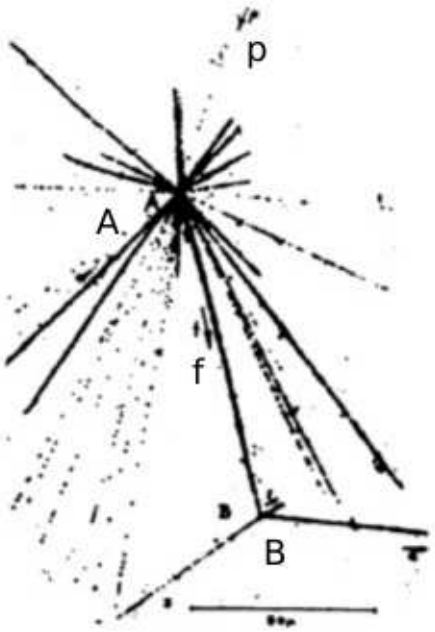

Fig. 1.1: The first hypernuclear decay observed. Incoming cosmic ray particle (track p) interacts with one of nuclei in the emulsion and a hypernucleus is produced (point A). Line f indicates the track of the hypernucleus which decays into three particles (point B) [1].

${}^{208}_{\Lambda}$Bi. The most precisely described hypernuclei are the lightest s- and p-shell Λ hypernuclei [7]. In addition, the following double-Λ hypernuclei have been measured in experiments: ${}^{\;\;6}_{\Lambda\Lambda}$He, ${}^{10}_{\Lambda\Lambda}$Be, and ${}^{13}_{\Lambda\Lambda}$B [8, 9, 10]. Except of Λ hypernuclei, only the bound system ${}^{4}_{\Sigma}$He was observed [11]. So far, there is no experimental evidence of Ξ and Ω hypernuclei.

The aim of this thesis is a theoretical description of single-particle spectra of Λ hypernuclei. We consider a hypernucleus as a many-body problem and, subsequently, we calculate its single-particle spectra using a mean-field approach. Mean field is constructed self-consistently by the Hartree-Fock method employing effective NN and ΛN interactions instead of purely phenomenological ones [12]. In this work, we implement two types of realistic NN interactions [13, 14]. The hypernuclear part is described by two effective ΛN potentials derived from the Nijmegen model [15, 16]. We do not implement directly three-body NNN forces. Instead, we add a density-dependent nucleon-nucleon (DDNN) interaction term to simulate their effect [17].

This work is organized as follows: Chapter 2 briefly introduces various theoretical approaches used in hypernuclear structure calculations, as well as our model. We present and discuss our results in Chapter 3. The main conclusions of this work, as well as future plans are given in Chapter 4. The harmonic oscillator basis and respective matrix elements used in our calculations are summarized in Appendix A.

Chapter 2

Hypernuclear many-body problem

Hypernuclear many-body problem consists in theoretical description of properties of hypernuclear many-body systems (i.e. systems of hyperons and nucleons) and solution of respective equations of motion. In general, the complete solution of quantum many-body problem is rather complex and up to now it has been done only for three-body (Fadeev equations) and four-body (Fadeev-Yakubovski equations) hypernuclear systems [18, 19, 20]. The main advantage of these calculations is that they use the free-space NN and ΛN interactions directly with the minimum of approximations.

Theoretical study of many-body systems with the mass number $A > 4$ is a complicated issue. Among many-body models which use realistic interactions belong for example No Core Shell Model [21, 22], Coupled Cluster Model [23], Fermionic Molecular Dynamics [24, 25], Self-Consistent Green's Function Method [26], and Green's Function Monte Carlo Model [27]. The main disadvantage of these models is that their computational complexity rapidly increases with the number of particles in the studied system. As a consequence, they are not commonly used for a description of hypernuclei above the sd-shell.

Heavier hypernuclei are studied within mean-field models [28]. Widely used is the Relativistic Mean Field (RMF) model [29, 30]. In this approach, the nucleons and hyperon are described as Dirac fields interacting via the exchange of meson fields. Another category of the mean-field models are those which use as an input phenomenological NN interactions as Skyrme [31, 32] and Gogny [33] potentials.

The applicability of the aforementioned models with respect to the size of the many-body system is not strictly defined. In general, the ab-initio models are used for description of systems with $A \geq 3$ and the mean-field models for $A > 10$.

Recently, the mean-field model constructed from realistic two-body nucleon-nucleon interactions was introduced and applied in ordinary nuclei [34], as well as hypernuclei [12].

2.1 Mean-field model based on realistic two-body baryon interactions

In our calculations, we describe a hypernucleus as a many-body system consisting of the nuclear core[1] and the Λ hyperon. Overall properties of the hypernucleus are given by the Hamiltonian

$$\widehat{H} = \widehat{T} + \widehat{V}^{\mathrm{NN}} + \widehat{V}^{\Lambda\mathrm{N}} - \widehat{T}_{\mathrm{CM}}, \tag{2.1}$$

where $\widehat{T}$ stands for the sum of kinetic energy operators of each nucleon and Λ, $\widehat{V}^{\mathrm{NN}}$ denotes the sum of the two-body NN potentials between any two nucleons, $\widehat{V}^{\Lambda\mathrm{N}}$ is the two-body potential between the Λ hyperon and each nucleon of the nuclear core, and $\widehat{T}_{\mathrm{CM}}$ is the center of mass kinetic energy of the hypernuclear system

$$\widehat{T}_{\mathrm{CM}} = \frac{1}{2MA}\left(\sum_{a=1}^{A}\widehat{\vec{P}}_a^{\,2} + \sum_{a<b}\widehat{\vec{P}}_a\cdot\widehat{\vec{P}}_b\right), \tag{2.2}$$

where indices a, b run over all baryons (i.e. the Λ hyperon and each nucleon of the nuclear core). The symbol M stands for the average mass of the proton and neutron. It is to be noted that while the mass difference of protons and neutrons is negligible, the Λ hyperon is heavier than the nucleon. However, the different mass of Λ is not considered in Eq. (2.2).

The nuclear core is described by self-consistent mean field constructed by the Hartree-Fock (HF) method. It is a microscopical approach in which the nuclear mean field is generated by averaging over all mutual NN interactions. These interactions can be either realistic or phenomenological. When the nuclear mean field is constructed the Λ particle is inserted into the nucleus. Then the equations of motion of the Λ hyperon are solved in the mean nuclear potential.

We intend to find the eigenvalues ε_i of the Hamiltonian (2.1) and the corresponding hypernuclear wave functions in the form

$$\Phi_i = \phi^{\mathrm{p}}(\vec{r}_1,\ldots,\vec{r}_Z)\cdot\phi^{\mathrm{n}}(\vec{r}\,'_1,\ldots,\vec{r}\,'_N)\cdot\psi_i^{\Lambda}(\vec{r}_\Lambda). \tag{2.3}$$

[1] By the term nuclear core we denote the subsystem of respective hypernucleus consisting only of protons and neutrons.

Here, the index i denotes the hypernuclear state. The wave function Φ_i is the product of proton ϕ^{p} and neutron ϕ^{n} parts obtained from the Hartree-Fock calculations, and the Λ single-particle wave functions ψ_i^{Λ}.

2.1.1 Hartree-Fock method

The starting point of this method is the following Hamiltonian for A identical particles

$$\widehat{H} = \sum_{a=1}^{A} \frac{\widehat{\vec{P}}_a^{\,2}}{2M} + \frac{1}{2} \sum_{a \neq b} \widehat{V}(\vec{r}_a, \vec{r}_b), \tag{2.4}$$

where $\widehat{T} = \sum_{a=1}^{A} \frac{\widehat{\vec{P}}_a^{\,2}}{2M}$ is the kinetic energy operator and $\widehat{V}(\vec{r}_a, \vec{r}_b)$ is the two-body potential acting between particles a and b.
The equations of motion are derived using the variational method

$$\delta \langle \phi | \widehat{H} | \phi \rangle = \langle \delta\phi | \widehat{H} | \phi \rangle = 0, \tag{2.5}$$

where ϕ is a many-body wave function of the considered system. Since we are dealing with nucleons, which are fermions, the antisymmetrization of the total wave function is obtained by the Slater determinant

$$\phi(\vec{r}_1, \vec{r}_2, \ldots, \vec{r}_A) = \frac{1}{\sqrt{A!}} \begin{vmatrix} \psi_1(\vec{r}_1) & \psi_2(\vec{r}_1) & \ldots & \psi_A(\vec{r}_1) \\ \psi_1(\vec{r}_2) & \psi_2(\vec{r}_2) & \ldots & \psi_A(\vec{r}_2) \\ \vdots & \vdots & \ddots & \vdots \\ \psi_1(\vec{r}_A) & \psi_2(\vec{r}_A) & \ldots & \psi_A(\vec{r}_A) \end{vmatrix}. \tag{2.6}$$

The single-particle wave functions ψ_i satisfy the normalization condition

$$\langle \psi_i | \psi_i \rangle = \int \mathrm{d}^3 r \; |\psi_i(\vec{r})|^2 = 1. \tag{2.7}$$

The energy functional $\langle \phi | \widehat{\mathrm{H}} | \phi \rangle$ is then defined as follows

$$\begin{aligned} \langle \phi | \widehat{H} | \phi \rangle = & - \frac{\hbar^2}{2M} \sum_{i=1}^{A} \int \mathrm{d}^3 r \; \psi_i^*(\vec{r}) \vec{\nabla}^2 \psi_i(\vec{r}) \\ & + \frac{1}{2} \sum_{ij}^{A} \iint \mathrm{d}^3 r \mathrm{d}^3 r' \; \psi_i^*(\vec{r}) \psi_j^*(\vec{r}\,') v(\vec{r}, \vec{r}\,') \psi_i(\vec{r}) \psi_j(\vec{r}\,') \\ & - \frac{1}{2} \sum_{ij}^{A} \iint \mathrm{d}^3 r \mathrm{d}^3 r' \; \psi_i^*(\vec{r}) \psi_j^*(\vec{r}\,') v(\vec{r}, \vec{r}\,') \psi_i(\vec{r}\,') \psi_j(\vec{r}). \end{aligned} \tag{2.8}$$

The variation of the energy functional (2.8) together with the normalization condition (2.7) yields the equation

$$\delta\left[\langle\phi|\widehat{H}|\phi\rangle-\varepsilon_i(\langle\psi_i|\psi_i\rangle-1)\right]=\frac{\partial}{\partial\psi_i^*}\left\{-\frac{\hbar^2}{2M}\sum_{i=1}^{A}\int \mathrm{d}^3r\ \psi_i^*(\vec{r})\vec{\nabla}^2\psi_i(\vec{r})\right.$$
$$+\frac{1}{2}\sum_{ij}^{A}\iint \mathrm{d}^3r\mathrm{d}^3r'\ \psi_i^*(\vec{r})\psi_j^*(\vec{r}\,')v(\vec{r},\vec{r}\,')\psi_i(\vec{r})\psi_j(\vec{r}\,')$$
$$-\frac{1}{2}\sum_{ij}^{A}\iint \mathrm{d}^3r\mathrm{d}^3r'\ \psi_i^*(\vec{r})\psi_j^*(\vec{r}\,')v(\vec{r},\vec{r}\,')\psi_i(\vec{r}\,')\psi_j(\vec{r})$$
$$\left.-\ \varepsilon_i\left(\int \mathrm{d}^3r\ \psi_i^*(\vec{r})\psi_i(\vec{r})-1\right)\right\}=0. \tag{2.9}$$

Eq. (2.9) can be after the partial derivation expressed as

$$-\frac{\hbar^2}{2M}\vec{\nabla}^2\psi_i(\vec{r})+\sum_{j=1}^{A}\int \mathrm{d}^3r'\ v(\vec{r},\vec{r}\,')\psi_j^*(\vec{r}\,')\psi_j(\vec{r}\,')\psi_i(\vec{r})$$
$$-\sum_{j=1}^{A}\int \mathrm{d}^3r'\ v(\vec{r},\vec{r}\,')\psi_j^*(\vec{r}\,')\psi_j(\vec{r})\psi_i(\vec{r}\,')=\varepsilon_i\psi_i(\vec{r}), \tag{2.10}$$

where ε_i are the single-particle energies. Again, Eq. (2.10) can be rewritten into the more elegant form

$$-\frac{\hbar^2}{2M}\vec{\nabla}^2\psi_i(\vec{r})+\int \mathrm{d}^3r'\ u(\vec{r},\vec{r}\,')\psi_i(\vec{r}\,')=\varepsilon_i\psi_i(\vec{r}), \tag{2.11}$$

where $u(\vec{r},\vec{r}\,')$ is the mean-field potential defined as

$$u(\vec{r},\vec{r}\,')=\delta(\vec{r}-\vec{r}\,')\sum_{j=1}^{A}\int \mathrm{d}^3r''\ v(\vec{r},\vec{r}\,'')\psi_j(\vec{r}\,'')\psi_j^*(\vec{r}\,'')$$
$$-\sum_{j=1}^{A}v(\vec{r},\vec{r}\,')\psi_j^*(\vec{r}\,')\psi_j(\vec{r}). \tag{2.12}$$

Second quantization

In our work, we use the HF method in a formalism of second quantization. In this formalism, the Hamiltonian (2.4) is rewritten in terms of creation and annihilation operators $a^\dagger$ and a, respectively

$$\widehat{H}=\sum_{ij}t_{ij}a_i^\dagger a_j+\frac{1}{4}\sum_{ijkl}V_{ijkl}^{\mathrm{NN}}a_i^\dagger a_j^\dagger a_l a_k, \tag{2.13}$$

Here, one-body and two-body operators are expressed as matrices where $t_{ij}=\langle i|\widehat{T}|j\rangle$ is the matrix element of the kinetic operator $\widehat{T}$ and V_{ijkl}^{NN} is the antisymmetrized

matrix element of the two-body operator $\widehat{V}^{\mathrm{NN}}$

$$V_{ijkl}^{\mathrm{NN}} = \langle ij|\widehat{V}^{\mathrm{NN}}|kl\rangle - \langle ij|\widehat{V}^{\mathrm{NN}}|lk\rangle = \langle ij|\widehat{V}^{\mathrm{NN}}|kl - lk\rangle.$$

Indices i, j, k, l represent single-particle states. The ground state A-body wave function can be expressed in terms of single-particle creation operators as

$$|\mathrm{HF}\rangle = \prod_{i=1}^{A} a_i^\dagger|0\rangle, \tag{2.14}$$

where $|0\rangle$ denotes the vacuum (i.e. a state without particles). The product in (2.14) runs over A lowest occupied states.
By using the variational principle

$$\delta\langle \mathrm{HF}|\widehat{H}|\mathrm{HF}\rangle = 0, \tag{2.15}$$

together with the Wick's theorem [35] the Hamiltonian (2.13) can be expressed as

$$\widehat{H} = \sum_{ij}\left\{ t_{ij} + \sum_{kl} V_{kilj}^{\mathrm{NN}}\langle \mathrm{HF}|a_k^\dagger a_l|\mathrm{HF}\rangle \right\} a_i^\dagger a_j \tag{2.16a}$$

$$- \frac{1}{2}\sum_{ijkl} V_{ijkl}^{\mathrm{NN}}\langle \mathrm{HF}|a_i^\dagger a_k|\mathrm{HF}\rangle\langle \mathrm{HF}|a_j^\dagger a_l|\mathrm{HF}\rangle \tag{2.16b}$$

$$+ \frac{1}{4}\sum_{ijkl} V_{ijkl}^{\mathrm{NN}} :a_i^\dagger a_j^\dagger a_l a_k: , \tag{2.16c}$$

where $:a_i^\dagger a_j^\dagger a_l a_k:$ denotes the normal ordering of operators $a_i^\dagger a_j^\dagger a_l a_k$. Eq. (2.16a) defines the matrix elements of the mean-field operator

$$h_{ij} = \left\{ t_{ij} + \sum_{kl} V_{kilj}^{\mathrm{NN}}\langle \mathrm{HF}|a_k^\dagger a_l|\mathrm{HF}\rangle \right\} = \delta_{ij}\varepsilon_i. \tag{2.17}$$

The expression in Eq. (2.16b) contributes to the total ground state energy E_{HF} of the system

$$E_{\mathrm{HF}} = \sum_{i=1}^{A}\varepsilon_i - \frac{1}{2}\sum_{ijkl} V_{ijkl}^{\mathrm{NN}}\langle \mathrm{HF}|a_i^\dagger a_k|\mathrm{HF}\rangle\langle \mathrm{HF}|a_j^\dagger a_l|\mathrm{HF}\rangle, \tag{2.18}$$

where ε_i are the single-particle energies. The last term in Eq. (2.16c) denotes the residual interactions between the nucleons and does not contribute to the ground state energy of the system.

The many-body problem is then solved iteratively by using the following algorithm:

1. Express the matrix elements t_{ij} and V^{NN}_{ijkl} in a single-particle basis defined by operators $a^\dagger_i, a_i$,

2. Calculate the matrix h_{ij} (2.17),

3. Diagonalize the matrix h_{ij} and obtain the new single-particle states defined by operators $a'^\dagger_i, a'_i$ and the new single-particle energies ε'_i

4. Use the new states as an input for the next iteration.

This loop is repeated until the convergence condition is fulfilled, i.e. when

$$|\varepsilon_i \ - \ \varepsilon'_i| \ < \ \delta,$$

where δ is a small number. We solve the respective equations of motion for protons and neutrons separately. The explicit calculations can be performed in an arbitrary single-particle basis. In our calculations, we adopt the spherical harmonic oscillator (HO) basis which is described in more detail in Appendix A.

2.1.2 Hypernuclear mean field

The part of the Hamiltonian (2.1) which describes the interaction of the Λ hyperon can be expressed in the formalism of second quantization as follows

$$\widehat{H}^\Lambda = \sum_{ij} t_{ij} c^\dagger_i c_j + \sum_{ijkl} V^{\Lambda\mathrm{N}}_{ijkl} a^\dagger_i c^\dagger_j c_l a_k, \tag{2.19}$$

where $a^\dagger_i(a_i)$ are nucleon creation (annihilation) operators and $c^\dagger_i(c_i)$ are creation (annihilation) operators of the Λ hyperon. First, we diagonalize the matrix (2.17) for both protons and neutrons separately and we obtain the following equations

$$t^{\mathrm{p}}_{ij} + u^{\mathrm{p}}_{ij} = \delta_{ij}\varepsilon^{\mathrm{p}}_i, \tag{2.20a}$$
$$t^{\mathrm{n}}_{ij} + u^{\mathrm{n}}_{ij} = \delta_{ij}\varepsilon^{\mathrm{n}}_i, \tag{2.20b}$$

where $\varepsilon^{\mathrm{p}}_i$ and $\varepsilon^{\mathrm{n}}_i$ are proton and neutron single-particle energies, respectively. The terms u_{ij} in Eqs. (2.20a) and (2.20b) are defined as

$$u^{\mathrm{p}}_{ij} = V^{\mathrm{pp}}_{ikjl}\rho^{\mathrm{p}}_{lk} + V^{\mathrm{pn}}_{ikjl}\rho^{\mathrm{n}}_{lk}, \tag{2.21a}$$
$$u^{\mathrm{n}}_{ij} = V^{\mathrm{nn}}_{ikjl}\rho^{\mathrm{n}}_{lk} + V^{\mathrm{pn}}_{kilj}\rho^{\mathrm{p}}_{lk}, \tag{2.21b}$$

where ρ^α_{lk} is proton and neutron density matrix

$$\rho^\alpha_{lk} = \langle \mathrm{HF}|a^\dagger_k a_l|\mathrm{HF}\rangle_\alpha, \quad \alpha = \mathrm{p}, \mathrm{n}. \tag{2.22}$$

Then the single-particle energies and wave functions of the Λ hyperon are obtained by solving the equation

$$t^{\Lambda}_{ij} + u^{\Lambda}_{ij} = \delta_{ij}\varepsilon^{\Lambda}_{i}, \tag{2.23}$$

where u^{Λ}_{ij} is defined as

$$u^{\Lambda}_{ij} = V^{\mathrm{p}\Lambda}_{kilj}\rho^{\mathrm{p}}_{lk} + V^{\mathrm{n}\Lambda}_{kilj}\rho^{\mathrm{n}}_{lk}. \tag{2.24}$$

We solve the equations of motion of Λ independently with the proton and neutron densities ρ^{p}_{lk} and ρ^{n}_{lk}, respectively obtained from the HF calculation of the nuclear core. The matrix elements t_{ij}, V^{NN}_{ijkl}, and $V^{\Lambda\mathrm{N}}_{ijkl}$ used in Eqs. (2.21a), (2.21b), and (2.23) are expressed in the spherical HO basis and described in more detail in Appendix A.

2.2 NN and ΛN interactions

The self-consistent mean field model used in this work is based on realistic NN interactions. We use the chiral next-to-next-to leading order NN potential $\mathrm{N^2LO_{opt}}$ [13]. This two-body potential is optimized to minimize the effect of three-body NNN interactions. Nevertheless, their effect is still non-negligible. It was demonstrated that the calculations performed purely with two-body NN interactions give unrealistic nuclear density distributions [12]. Due to this fact, we add a density dependent NN interaction (DDNN) term [17]

$$\widehat{V}^{\mathrm{NN,DD}} = \frac{C_\rho}{6}(1 + \widehat{P}_\sigma)\rho\left(\frac{\vec{r}_1 + \vec{r}_2}{2}\right)\delta(\vec{r}_1 - \vec{r}_2) \tag{2.25}$$

to the Hamiltonian (2.1) which simulates the effect of NNN forces. Here, C_ρ is the coupling constant which enters the DDNN term as a free parameter. The symbol $\widehat{P}_\sigma = \frac{1}{2}(\mathbb{I} + \vec{\sigma}_1 \cdot \vec{\sigma}_2)$ denotes the spin exchange operator.

To describe the ΛN interaction we adopt the G-matrix transformed (YNG) potentials derived from the Nijmegen model ESC08a [16] and ESC08c [15]. The central part of the YNG ΛN interaction is given in a Gaussian form

$$G(r; k_{\mathrm{F}}) = \sum_{i=1}^{3}(a_i + b_i k_{\mathrm{F}} + c_i k_{\mathrm{F}}^2)\exp\left(-\frac{r^2}{\beta_i^2}\right), \tag{2.26}$$

where a_i, b_i, c_i, and β_i are real parameters and k_{F} is the Fermi momentum which simulates the properties of G-matrix in the nuclear medium. Besides the central part, the ΛN interaction contains the symmetric and antisymmetric spin-orbit terms which are included in our calculations as well. They are described in detail in

Ref. [16].

The Fermi momentum $k_{\rm F}$ can be either considered as a free parameter or it can be fixed by the Thomas-Fermi approximation

$$k_{\rm F} = \left(\frac{3\pi^2}{2} \langle \rho \rangle \right)^{1/3}, \tag{2.27}$$

where $\langle \rho \rangle$ is defined by the Average Density Approximation (ADA) [16]

$$\langle \rho \rangle = \int {\rm d}^3 r \; \rho_{\rm N}(\vec{r}) \rho_{\Lambda}(\vec{r}). \tag{2.28}$$

Here, $\rho_N(\vec{r})$ is the nuclear density distribution and $\rho_{\Lambda}(\vec{r})$ is the Λ density distribution. The Fermi momentum $k_{\rm F}$ is evaluated self-consistently in our calculations.

Chapter 3

Results

In this work, we study the spectra of the Λ hyperon bound in ^{16}O, ^{40}Ca, and ^{208}Pb. These nuclei are doubly-magic and spherically symmetric which makes them suitable for calculations in our model. In this chapter, we present all possible Λ single-particle energy states in a given basis – single-particle states with both positive and negative energies. The negative energy states represent actual Λ bound states and are the main subject of this thesis. The states with positive energy are possible excitations of the Λ hyperon and have further applications in beyond mean-field calculations [36]. In our study, we neglect the core polarization effects and $\Lambda - \Sigma$ mixing [37]. Throughout this work we use the notation ${}^{A}_{\Lambda}X$ for a nucleus X with a mass number A containing one Λ particle.

We employ the chiral $\mathrm{N^2LO_{opt}}$ [13] NN interaction to derive the nuclear mean field in our calculations. We use the effective YNG ΛN interaction derived from the Nijmegen model ESC08c [15] to describe the interaction of Λ hyperon with the nuclear mean field.

In order to calculate the hypernuclear spectra, we first need to describe correctly the nuclear core. It is due to the fact that the ΛN interaction depends on the Fermi momentum k_{F} which is a function of nuclear density (see Eq. (2.27)). The Hartree-Fock calculations performed exclusively with the two-body NN interaction do not give correct nuclear density distributions and, consequently, the Root Mean Square (RMS) radii. The nuclear density distribution is unreasonably compressed and yields much smaller RMS radii than are the experimental values [12]. Therefore, we add the phenomenological density-dependent DDNN interaction term (see Eq. (2.25)) to obtain reasonable nuclear density distributions.

The RMS radius is defined as

$$r_\alpha = \sqrt{\langle r^2 \rangle_\alpha} = \sqrt{\int \mathrm{d}^3 r \; r^2 \rho_\alpha(\vec{r})}, \tag{3.1}$$

where $\rho_\alpha(\vec{r})$ is a density distribution of either protons ($\alpha = \mathrm{p}$) or neutrons ($\alpha = \mathrm{n}$). The quantity measured in experiments is the proton charge radius r_{ch} related to r_{p} as follows

$$r_{\mathrm{ch}} = \sqrt{\langle r^2 \rangle_{\mathrm{p}} + q^2}, \tag{3.2}$$

where q^2 is the proton form factor, $q^2 = 0.64$ fm^2 [38]. First, we compare the nuclear density distributions calculated with the realistic NN interaction with results of the Relativistic Mean Field (RMF) model [29], a phenomenological model fitted to reproduce bulk properties of selected nuclei.

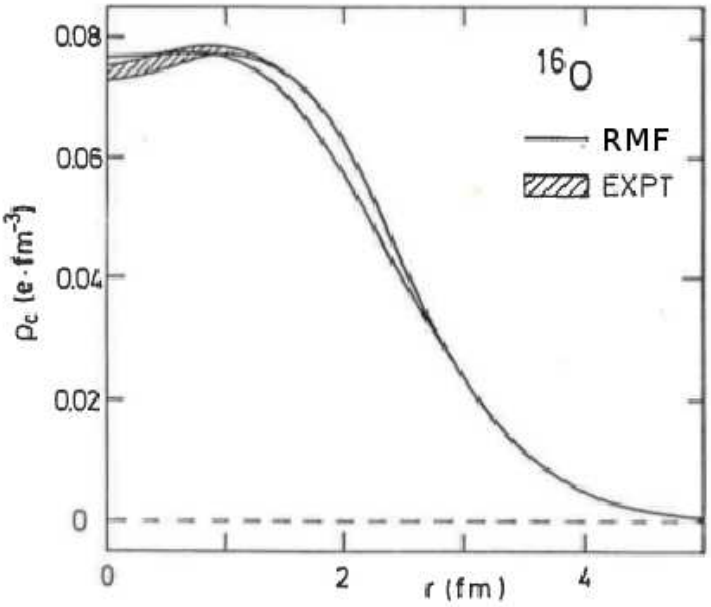

Fig. 3.1: The measured charge density distribution ρ_{ch} (EXPT) [38] in ^{16}O compared with the result of the RMF model.

In Fig. 3.1, there is a comparison of the measured charge density distribution in ^{16}O with the results of the RMF model. We fit the coupling constant C_ρ of the DDNN interaction term to the RMF nuclear density distributions in ^{16}O, ^{40}Ca, and ^{208}Pb to obtain reasonable density distributions and RMS radii. The results for C_ρ together with corresponding charge radii r_{ch} and experimental values $r_{\mathrm{ch}}^{\mathrm{exp}}$ are shown in Table 3.1. Our calculations are performed with the basis parameters $\mathrm{N}_{\mathrm{max}} = 10$ and $\hbar\omega = 16, 12$, and 8 MeV for ^{16}O, ^{40}Ca, and ^{208}Pb, respectively. The parameters $\mathrm{N}_{\mathrm{max}}$ and $\hbar\omega$ are described in detail in Appendix A.

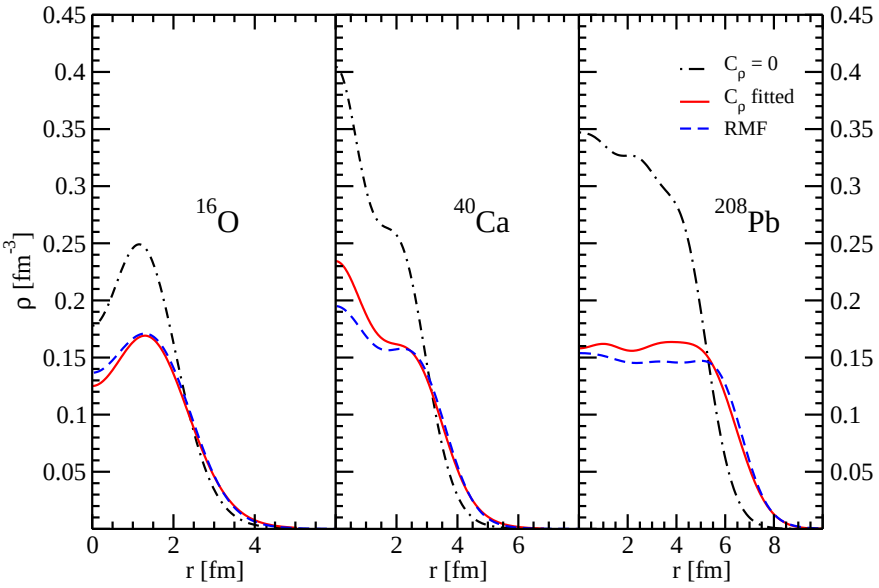

Fig. 3.2: The nuclear density distributions in ^{16}O, ^{40}Ca, and ^{208}Pb calculated within the RMF model (dashed line) compared with our results calculated with C_ρ from Table 3.1 (solid line) and with $C_\rho = 0$ (dash-dotted line).

In Fig. 3.2, we compare the nuclear density distributions calculated with C_ρ from Table 3.1 in ^{16}O, ^{40}Ca, and ^{208}Pb with the respective RMF density distributions. We present the nuclear density distributions calculated with $C_\rho = 0$ as well to show the importance of the DDNN interaction term. The nuclear density distributions calculated with the fitted values of the coupling constant C_ρ are in a good agreement with those calculated within the RMF model whereas the nuclear density distributions calculated without the DDNN term ($C_\rho = 0$) are unrealistic.

The correct nuclear density distributions are used to obtain the Fermi momenta

Table 3.1: The fitted values of the coupling constants C_ρ and corresponding charge radii $r_{\rm ch}$ in ^{16}O, ^{40}Ca, and ^{208}Pb compared with the experimental values $r_{\rm ch}^{\rm exp}$ [39].

	C_ρ [MeV·fm^6]	$r_{\rm ch}$ [fm]	$r_{\rm ch}^{\rm exp}$ [fm]
^{16}O	1600	2.72	2.70
^{40}Ca	2100	3.48	3.48
^{208}Pb	3300	5.47	5.50

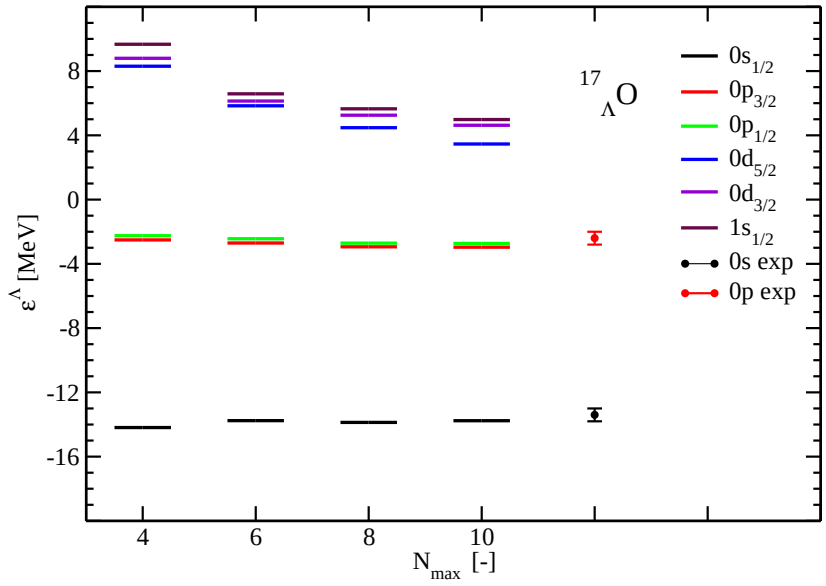

Fig. 3.3: The Λ single-particle energies ε^{Λ} in $^{17}_{\Lambda}$O as a function of N_{max}. Experimental data [40] are shown as filled circles with error bars for comparison.

k_F for each hypernucleus considered (see Eq. (2.27)). The results for k_F are shown in Table 3.2.

In Fig. 3.3 and 3.4, the Λ single-particle energies in $^{17}_{\Lambda}$O and $^{41}_{\Lambda}$Ca are shown as a function of N_{max}. The parameter $\hbar\omega$ is fixed to 16 MeV in $^{17}_{\Lambda}$O and 12 MeV in $^{41}_{\Lambda}$Ca. States with the negative energy exhibit fast convergence with respect to N_{max} in both hypernuclei and are in a good agreement with experimental data. Positive energy states do not converge. This issue is beyond the scope of this thesis and we do not discuss it further. In Fig. 3.5 and 3.6, we present the Λ single-particle energies in $^{17}_{\Lambda}$O and $^{41}_{\Lambda}$Ca as a function of $\hbar\omega$, calculated for fixed value of $N_{max} = 10$. We can see that the converged states with negative energies remain almost constant and do not depend on the choice of $\hbar\omega$ for $\hbar\omega > 6$ MeV.

Table 3.2: The values of Fermi momentum k_F in $^{17}_{\Lambda}$O, $^{41}_{\Lambda}$Ca, and $^{209}_{\Lambda}$Pb.

hypernucleus	$^{17}_{\Lambda}$O	$^{41}_{\Lambda}$Ca	$^{209}_{\Lambda}$Pb
k_F [fm^{-1}]	1.20	1.29	1.33

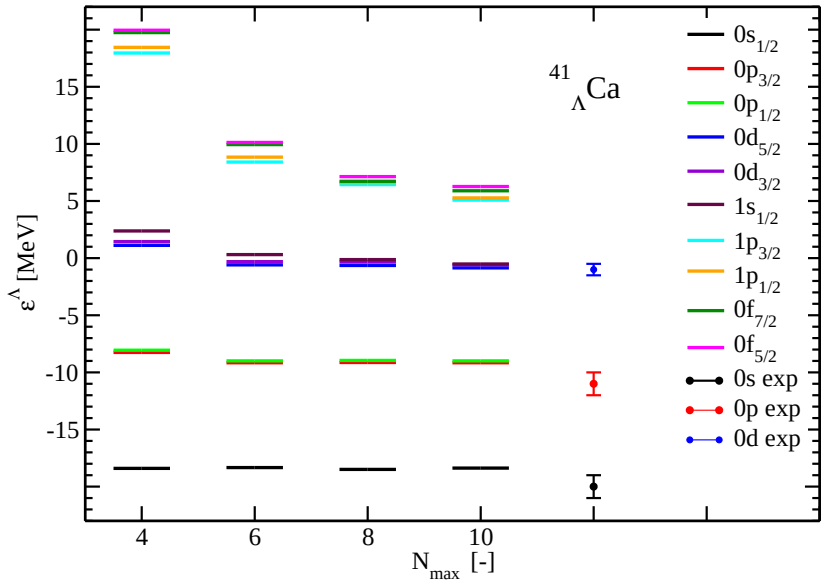

Fig. 3.4: The Λ single-particle energies ε^{Λ} in $^{41}_{\Lambda}$Ca as a function of N_{max}. Experimental data [41] are shown as filled circles with error bars for comparison.

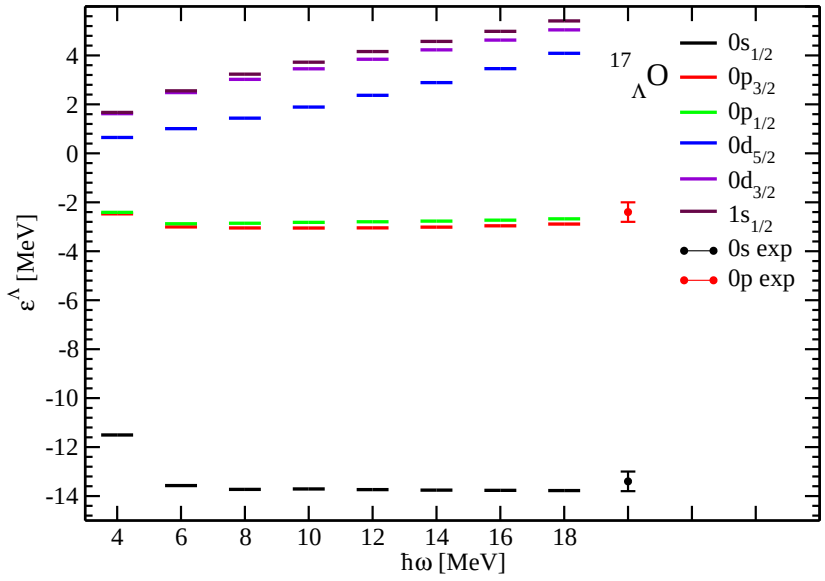

Fig. 3.5: The Λ-single particle energies ε^{Λ} in $^{17}_{\Lambda}$O as a function of $\hbar\omega$. Experimental data [40] are shown as filled circles with error bars for comparison.

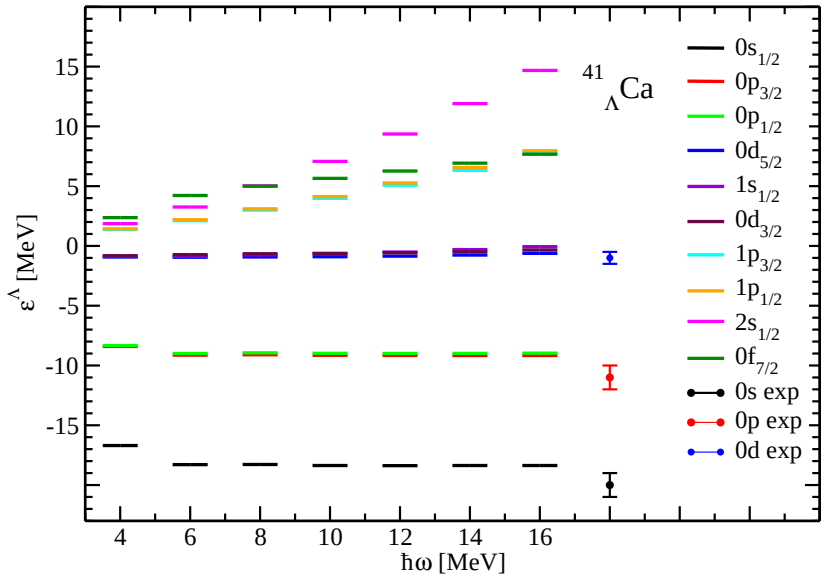

Fig. 3.6: The Λ single-particle energies ε^{Λ} in $^{41}_{\Lambda}$Ca as a function of $\hbar\omega$. Experimental data [41] are shown as filled circles with error bars for comparison.

Next, we explore the dependence of Λ single-particle spectrum on the choice of NN and ΛN interaction in order to study the potential model dependence of our calculations. In Fig. 3.7, we compare the Λ single-particle energies in $^{17}_{\Lambda}$O calculated with different choices of NN and ΛN interactions. We use the NN interactions N^{2}LO$_{\rm opt}$ and CD-Bonn+V$_{\rm low-k}$ [14] with cut-off parameter $\lambda = 2.6$ fm^{-1} and the YNG ΛN interactions derived from the ESC08 model – ESC08a and ESC08c [16, 15]. We include the DDNN term into the CD-Bonn NN interaction as well, and fit the value of the coupling constant C_ρ again to obtain the nuclear density distribution consistent with the RMF model. We get the same value of the coupling constant $C_\rho = 1600$ MeV·fm^6 as in the case of the N^{2}LO$_{\rm opt}$ NN interaction. The corresponding value of the Fermi momentum is $k_{\rm F} = 1.20$ fm^{-1}. We present our result for the following combinations of the NN and ΛN interactions:

(i.) N^{2}LO$_{\rm opt}$ + YNG-Force (ESC08c),

(ii.) N^{2}LO$_{\rm opt}$ + YNG-Force (ESC08a),

(iii.) CD-Bonn + YNG-Force (ESC08a),

(iv.) CD-Bonn + YNG-Force (ESC08c).

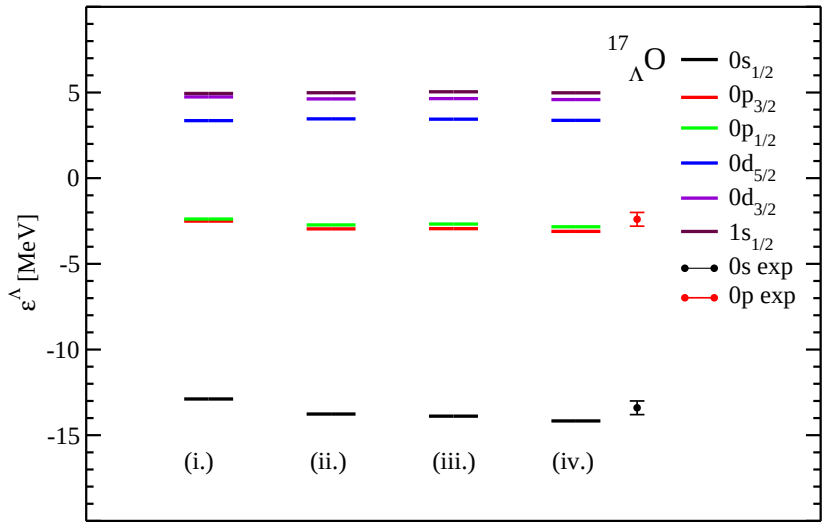

Fig. 3.7: The Λ single-particle energies ε^{Λ} in $^{17}_{\Lambda}$O calculated for various combinations of NN and ΛN interactions (i.), (ii.), (iii.), and (iv.) (see text for details). Experimental data [40] are shown as filled circles with error bars for comparison.

The Λ single-particle energies calculated for different combinations of NN and ΛN interactions do not deviate much from each other and correspond with the experimental data.

We study the influence of the DDNN interaction term on Λ single-particle spectrum as well. We performed calculations of the Λ single-particle energies in $^{41}_{\Lambda}$Ca with $N_{max} = 10$ and $\hbar\omega = 12$ MeV for the following combinations of C_ρ and k_F:

(i.) $C_\rho = 2100$ MeV·fm^6, $k_F = 1.29$ fm^{-1},

(ii.) $C_\rho = 0$, $k_F = 1.29$ fm^{-1},

(iii.) $C_\rho = 0$, $k_F = 1.49$ fm^{-1}.

In the case (i.), the coupling constant C_ρ is fitted to match the RMF nuclear density distribution in ^{40}Ca. Its value is $C_\rho = 2100$ MeV·fm^6. The Fermi momentum $k_F = 1.29$ fm^{-1} is calculated for this particular choice of C_ρ. In calculation (ii.), we set the coupling constant $C_\rho = 0$ and leave the value of the Fermi momentum $k_F = 1.29$ fm^{-1} from calculation (i.). In (iii.), the new value of the Fermi momentum $k_F = 1.49$ fm^{-1} is calculated in order to be consistent with the nuclear density distribution for $C_\rho = 0$.

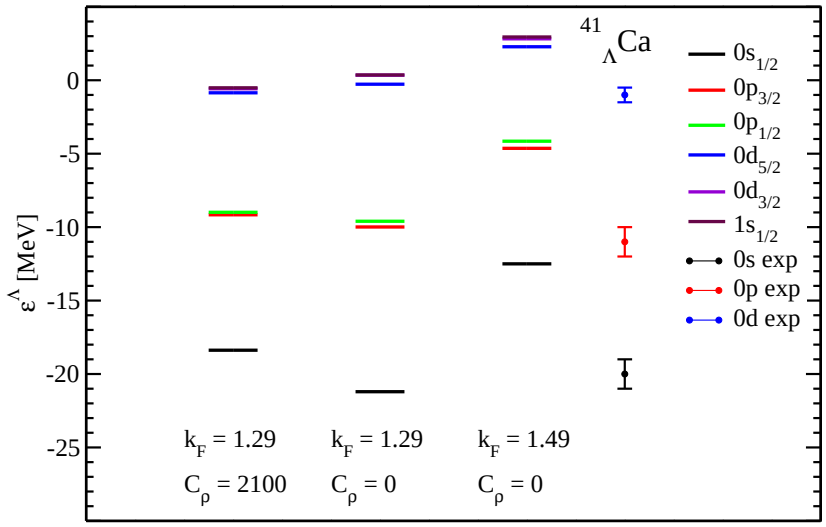

Fig. 3.8: The Λ single-particle energies ε^{Λ} in $^{41}_{\Lambda}$Ca calculated for different values of C_ρ and $k_{\rm F}$ (see text for details). Experimental data [41] are shown as filled circles with error bars for comparison.

The results of these calculations are presented in Fig. 3.8. The Λ single-particle energies calculated in (i.) are in agreement with available experimental data. The Λ single-particle energies calculated in (ii.) yield larger gaps between the 0s, 0p, and 0d levels, as well as unrealistic spin-orbit splitting of 0p and 0d levels [30]. The Λ single-particle energies calculated in (iii.) are shifted upwards with respect to previous calculations (i.) and (ii.), and do not correspond with experimental data.

In Fig. 3.9, the Λ single-particle energies in $^{209}_{\Lambda}$Pb are shown as a function of $\hbar\omega$. The results are very unstable even for the negative energy states and vary significantly with $\hbar\omega$. In order to examine this issue, we first check the nuclear density distribution for each $\hbar\omega$ considered.

In Fig. 3.10, we show the comparison of nuclear density distributions in studied nuclei calculated for various $\hbar\omega$ with the RMF density distributions. The nuclear density distributions in ^{16}O and ^{40}Ca do not deviate much from each other for different $\hbar\omega$ (except $\hbar\omega = 4$ MeV). However, the nuclear density distribution in ^{208}Pb changes drastically with $\hbar\omega$.

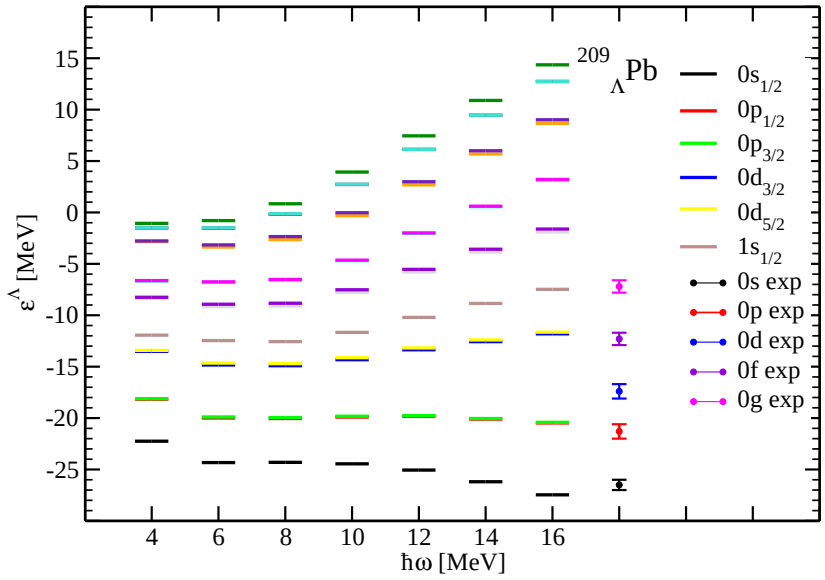

Fig. 3.9: The Λ single-particle energies ε^{Λ} in $^{209}_{\Lambda}$Pb as a function of $\hbar\omega$. Experimental data [42] are shown as filled circles with error bars for comparison.

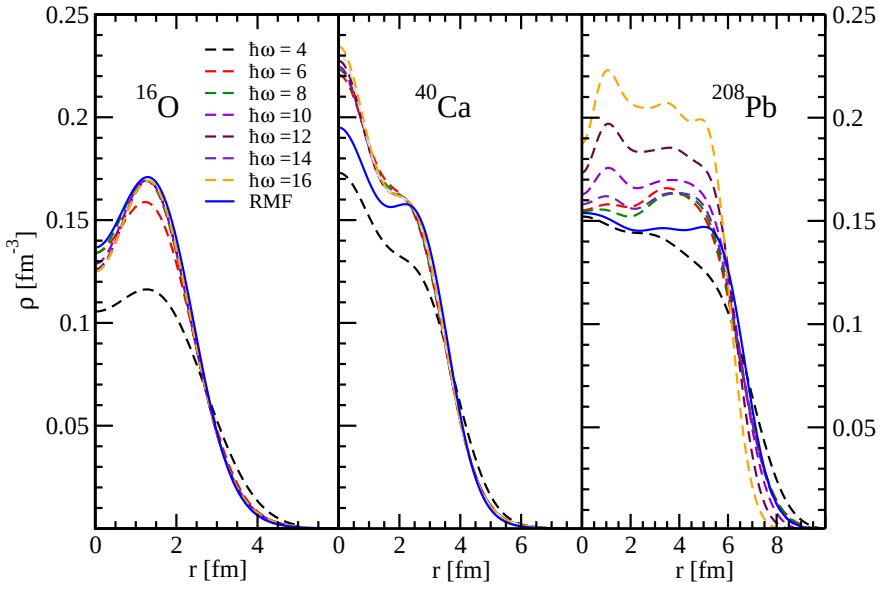

Fig. 3.10: The nuclear density distributions in ^{16}O, ^{40}Ca, and ^{208}Pb calculated for various $\hbar\omega$ (dashed lines) compared with the RMF density distributions (solid lines).

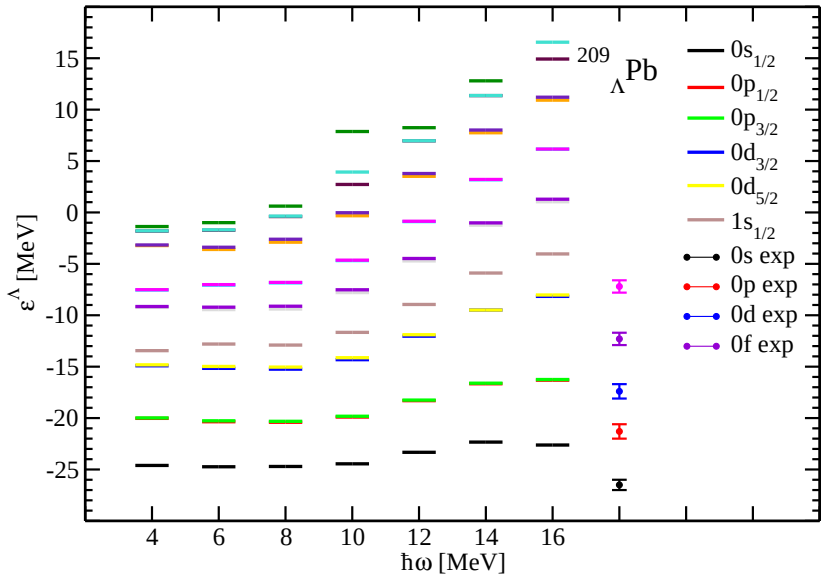

Fig. 3.11: The Λ single-particle energies ε^{Λ} in ${}^{209}_{\Lambda}$Pb calculated with the coupling constants C_ρ and Fermi momenta k_{F} from Table 3.3 as a function of $\hbar\omega$. Experimental data [42] are shown as filled circles with error bars for comparison.

To stabilize the Λ single-particle spectrum in ${}^{209}_{\Lambda}$Pb with respect to parameter $\hbar\omega$ we fit the coupling constant C_ρ for each $\hbar\omega$ separately. We calculate the new values of the Fermi momenta k_{F} which correspond to the fitted values of C_ρ for each $\hbar\omega$. The results are shown in Table 3.3. With these new parameters we calculate the Λ single-particle energies for each $\hbar\omega$ and present them in Fig. 3.11. The Λ single-particle energies calculated with refitted values of C_ρ still depend considerably on the model parameter $\hbar\omega$. This problem occurs due to the small size of the single-particle basis for ${}^{209}_{\Lambda}$Pb. The convergence of single-particle spectra in the Hartree-Fock method depends on the number of unoccupied major shells. For $\mathrm{N_{max}} = 10$ there are only 4 unoccupied major shells for neutrons and 5 unoccupied major shells for protons in ${}^{209}_{\Lambda}$Pb. This number of unoccupied major shells is not sufficient to reach the convergence in ${}^{209}_{\Lambda}$Pb.

Table 3.3: The fitted values of coupling constant C_ρ and corresponding values of $k_{\rm F}$ in ${}^{209}_{\Lambda}$Pb for each $\hbar\omega$.

$\hbar\omega$ [MeV]	k_F [fm^{-1}]	C_ρ [MeV·fm^6]
4	1.30	2200
6	1.32	3300
8	1.32	3300
10	1.33	3300
12	1.34	4300
14	1.38	5300
16	1.38	7300

Chapter 4

Conclusions

In this work, we studied the properties of the Λ single-particle spectra in ${}^{17}_{\Lambda}$O, ${}^{41}_{\Lambda}$Ca, and ${}^{209}_{\Lambda}$Pb. We used the Hartree-Fock method in the HO basis to generate a nuclear mean field from the realistic NN interaction N^2LO_{opt}. The phenomenological DDNN interaction term was included to describe correctly the nuclear density distributions in considered nuclei. We fitted the coupling constant C_ρ of the DDNN interaction term to match the nuclear density distributions in ^{16}O, ^{40}Ca and ^{208}Pb with the results of the Relativistic Mean-Field model. The ΛN interaction was described by the YNG interaction model ESC08 in which the Fermi momentum entered as a free parameter. We fixed the value of the Fermi momentum k_F for each studied hypernucleus via the Thomas-Fermi approximation.

We studied the dependence of the Λ single-particle energies ε^Λ in ${}^{17}_{\Lambda}$O and ${}^{41}_{\Lambda}$Ca on the basis parameters N_{max} and $\hbar\omega$. We found that the negative energy states had converged rather fast and did not depend much on the basis parameters N_{max} and $\hbar\omega$.

We performed calculations of the Λ single-particle spectra in the ${}^{17}_{\Lambda}$O with different choices of NN and ΛN interactions. We considered two types of NN interactions: N^2LO_{opt} and CD-Bonn+V_{low-k}, as well as two ΛN interactions ESC08c and ESC08a. The calculated Λ single-particle spectra did not change significantly with different NN and ΛN potential models.

We explored the dependence of the Λ single-particle energies ε^Λ in ${}^{41}_{\Lambda}$Ca on the coupling constant C_ρ and the Fermi momentum k_F. First, we calculated the spectrum for $C_\rho = 2100$ MeV·fm^6, the value fitted to reproduce the RMF nuclear density distribution in ^{40}Ca, and for corresponding $k_F = 1.29$ fm^{-1} calculated using the Thomas-Fermi approximation. The results were in a good agreement with experimental data. Next, we set $C_\rho = 0$ and left the Fermi momentum from previous calculation, $k_F = 1.29$ fm^{-1}. We observed larger gaps between 0s, 0p, and 0d lev-

els, as well as larger spin-orbit splitting of 0p and 0d levels. Then we set $C_\rho = 0$ and calculated the relevant value of $k_{\mathrm{F}} = 1.49$ fm^{-1}. The results were substantially shifted with respect to the previous two cases and did not correspond with available experimental data.

We studied the dependence of Λ single-particle energies ε^{Λ} in ${}^{209}_{\Lambda}$Pb on the parameter $\hbar\omega$ as well. We discovered that the Λ single-particle energies were unstable and varied considerably with $\hbar\omega$. We found that the nuclear density distribution in ^{208}Pb differed drastically for each $\hbar\omega$ considered whereas the nuclear density distributions in ^{16}O and ^{40}Ca remained very similar to each other for different $\hbar\omega$. Therefore, we fitted the coupling constant C_ρ for each $\hbar\omega$ independently and calculated respective values of the Fermi momenta. However, the Λ single-particle energies remained unstable with respect to $\hbar\omega$. We concluded that the size of the basis for $\mathrm{N_{max}} = 10$ was not sufficient to reach the convergence of the Λ single-particle states in ${}^{209}_{\Lambda}$Pb.

In our work, we discovered that the self-consistent mean-field model based on the chiral NN and YNG ΛN interaction derived from the Nijmegen model had several drawbacks and would need further improvements. Calculations in our basis were restricted due to its limited size. The largest available basis was for $\mathrm{N_{max}} = 10$ since the calculations with larger $\mathrm{N_{max}}$ were not feasible in the current version of our code due to the computational complexity. Consequently, our basis was too small to reach the convergence in ${}^{209}_{\Lambda}$Pb. Therefore, it would be desirable to perform the calculations for larger $\mathrm{N_{max}}$.

Next, we did not implement the three-body NNN interactions directly but we simulated their effect with the phenomenological DDNN interaction term. In future, we plan to introduce the chiral $\mathrm{N^2LO}$ NNN interaction which is consistent with the chiral $\mathrm{N^2LO_{opt}}$ NN interaction. It will be desirable to employ other realistic ΛN interaction as well, such as those derived from the Effective Field Theory [43].

We plan to take into account $\Lambda - \Sigma$ mixing and effect of the ΛNN interaction in our future calculations. In addition, we aim to study the core polarization effects and correlations from the beyond mean-field configurations.

Moreover, we would like to use our model in deformed single-particle basis. This will allow us to study hypernuclei with nuclear cores that do not have doubly-closed shells.

Appendix A

Matrix elements in spherical harmonic oscillator basis

The spherical harmonic oscillator basis consists of the single-particle states denoted by quantum numbers n, l, j, and m, where n is the major quantum number, l is the orbital angular momentum, j is the total angular momentum, and m is the projection of total angular momentum. The quantum numbers l, j, and m satisfy the following relations

$$\left| l - \frac{1}{2} \right| \leq \ j \ \leq l + \frac{1}{2}, \tag{A.1a}$$

$$m = -j, -j+1, \ldots, j-1, j. \tag{A.1b}$$

The energy of a given state is defined as

$$E_{nl} = \hbar\omega \left(\underbrace{2n + l}_{\mathrm{N}} + \frac{3}{2} \right), \tag{A.2}$$

where we define the number of the major shell N. The size of the basis is determined by the maximal major shell number $\mathrm{N}_{\max}$, i.e. the basis is spanned by the major shells $\mathrm{N} = 0, 1, \ldots, \mathrm{N}_{\max}$. Another parameter of HO basis is $\hbar\omega$ - the oscillator frequency which determines the width of the oscillator potential well.

The single-particle wave function of a state denoted by quantum numbers n, l, j, m is defined as

$$\psi_{nljm} = R_{nl}(r, b) \cdot \left[Y_l(\varphi, \Omega) \otimes \chi_{\frac{1}{2}} \right]_{jm}, \tag{A.3}$$

where $Y_l(\varphi, \Omega)$ is the spherical harmonics, $\chi_{\frac{1}{2}}$ is spinor both coupled in the total angular momentum j and its projection m. Radial wave function $R_{nl}(r, b)$ is defined as

$$R_{nl}(r, b) = b^{3/2} \sqrt{\frac{2n!}{(n + l + \frac{1}{2})!}} (br)^l L_n^{(l+\frac{1}{2})}(b^2 r^2) \mathrm{e}^{-\frac{b^2 r^2}{2}}, \tag{A.4}$$

where $L_n^{(l+\frac{1}{2})}(b^2r^2)$ is the Laguerre polynomial and b is the inverse oscillator length

$$b = \sqrt{\frac{M_B c^2 \hbar\omega}{\hbar^2 c^2}}, \quad B = N, \Lambda. \tag{A.5}$$

The matrix elements t_{ij} in the Hamiltonians (2.13), (2.19) are defined as

$$\begin{aligned} t_{ij} = \left(1-\frac{1}{A}\right)\left\langle n_i l_i j_i m_i \left| \frac{\widehat{\vec{P}}^2}{2M_B} \right| n_j l_j j_j m_j \right\rangle = \\ \left(1-\frac{1}{A}\right)\left[\frac{1}{2}\hbar\omega\left(2n_i + l_i + \frac{3}{2}\right)\delta_{n_i n_j}\delta_{l_i l_j}\delta_{j_i j_j}\delta_{m_i m_j}\right. \\ + \frac{1}{2}\hbar\omega\sqrt{n_i\left(n_i + l_i + \frac{1}{2}\right)}\delta_{n_i n_j+1}\delta_{l_i l_j}\delta_{j_i j_j}\delta_{m_i m_j} \\ \left. + \frac{1}{2}\hbar\omega\sqrt{n_j\left(n_j + l_j + \frac{1}{2}\right)}\delta_{n_i+1 n_j}\delta_{l_i l_j}\delta_{j_i j_j}\delta_{m_i m_j}\right]. \end{aligned} \tag{A.6}$$

The right side of Eq. (A.6) do not depend on the mass of considered particle. However, the different mass of Λ has to be taken into account in the inverse oscillator length (A.5) which enters the radial wave function (A.4).

The antisymetric matrix element $V_{ijkl}^{\rm NN}$ in Eq. (2.13) is expressed as

$$V_{ijkl}^{\rm NN} = \left\langle ij \left| \widehat{V}^{\rm NN} + \widehat{V}^{\rm NN,DD} - \frac{\widehat{\vec{P}}_1 \cdot \widehat{\vec{P}}_2}{2MA} \right| kl - lk \right\rangle, \tag{A.7}$$

where $\widehat{V}^{\rm NN}$ stands for the realistic NN interaction and $\widehat{V}^{\rm NN,DD}$ is the DDNN term (2.25). The matrix elements of the NN interaction operator $\langle ij|\widehat{V}^{\rm NN}|kl-lk\rangle$, as well as the antisymmetrized matrix elements $\langle ij|\frac{\widehat{\vec{P}}_1\cdot\widehat{\vec{P}}_2}{2M}|kl-lk\rangle$ are generated by the CENS code [44] and we do not show them explicitly. The matrix elements of the DDNN term $\langle ij|\widehat{V}^{\rm NN,DD}|kl-lk\rangle$ are defined as

$$\begin{aligned} &\langle ij|\widehat{V}^{\rm NN,DD}|kl-lk\rangle = \\ &= \langle n_i l_i j_i m_i, n_j l_j j_j m_j|\widehat{V}^{\rm NN,DD}|n_k l_k j_k m_k, n_l l_l j_l m_l - n_l l_l j_l m_l, n_k l_k j_k m_k\rangle \\ &= \sum_J C^{Jm_i+m_j}_{j_i m_i j_j m_j} C^{Jm_k+m_l}_{j_k m_k j_l m_l} V_{ijkl}^{\rm DD,NN;J}, \end{aligned} \tag{A.8}$$

where $C^{Jm_i+m_j}_{j_i m_i j_j m_j}$ are the Clebsh-Gordan coefficients. The matrix elements $V_{ijkl}^{\rm DD,NN;J}$ are non-zero only for proton-neutron interaction

$$\begin{aligned} V_{ijkl}^{\rm DD,pn;J} = \frac{C_\rho}{4\pi}\frac{1}{24(2J+1)}\sqrt{(2j_i+1)(2j_j+1)(2j_k+1)(2j_l+1)}I_{rad} \\ [2(-1)^{j_i+j_j+j_k+j_l}(1+(-1)^{l_i+l_j+l_k+l_l})C^{J1}_{j_i 1/2 j_j 1/2}C^{J1}_{j_k 1/2 j_l 1/2} \\ -(-1)^{l_i+l_k+j_i+j_k}(1-(-1)^{J+l_i+l_j})(1-(-1)^{J+l_k+l_l})C^{J0}_{j_i 1/2 j_j -1/2}C^{J0}_{j_k 1/2 j_l -1/2}]. \end{aligned} \tag{A.9}$$

In Eq. (A.9), we use the radial integral I_{rad}

$$I_{rad} = \int \mathrm{d}^3 r \; \rho(\vec{r}) R_{n_i l_i}(r,b) R_{n_j l_j}(r,b) R_{n_k l_k}(r,b) R_{n_l l_l}(r,b). \tag{A.10}$$

The symmetric matrix element $V^{\Lambda\mathrm{N}}_{ijkl}$ in Eq. (2.19) is expressed as

$$V^{\Lambda\mathrm{N}}_{ijkl} = \left\langle ij \left| \widehat{V}^{\Lambda\mathrm{N}} - \frac{\widehat{\vec{P}}_1 \cdot \widehat{\vec{P}}_2}{2MA} \right| kl \right\rangle, \tag{A.11}$$

where the symmetrized matrix elements $\langle ij|\frac{\widehat{\vec{P}}_1 \cdot \widehat{\vec{P}}_2}{2M}|kl\rangle$ are generated by the CENS code [44]. The ΛN interaction in Eq. (2.26) is expressed in the form of one-body matrix elements $\langle n_1 l_1, S|G(r;k_{\mathrm{F}})|n_2 l_2, S\rangle$

$$\begin{aligned} &\langle n_1 l_1, S|G(r;k_{\mathrm{F}})|n_2 l_2, S\rangle = \\ &= \left[\chi_i^\dagger \otimes \chi_j^\dagger\right]_S 4\pi \int r^2 \mathrm{d}r \; R_{n_1 l_1}(r, b_{\mathrm{rel}}) G(r;k_{\mathrm{F}}) R_{n_2 l_2}(r, b_{\mathrm{rel}}) \left[\chi_k \otimes \chi_l\right]_S, \end{aligned} \tag{A.12}$$

where χ_i represents spinor of the i-th particle and $R_{nl}(r, b_{\mathrm{rel}})$ are the radial wave functions (A.4) expressed in the relative coordinates. Their oscillator length b_{rel} is given as follows

$$b_{\mathrm{rel}} = \frac{b}{\sqrt{1 + \frac{M_N}{M_\Lambda}}} \approx \frac{b}{\sqrt{1.84}}, \tag{A.13}$$

where $M_N \approx 938$ MeV is the nucleon mass and $M_\Lambda \approx 1115$ MeV is the mass of the Λ hyperon. The two-body matrix elements $\langle ij|\widehat{V}^{\Lambda\mathrm{N}}|kl\rangle$ are obtained from the elements in Eq. (A.12) by the transformation introduced in [45].

Bibliography

[1] M. Danysz, J. Pniewski, Phil. Mag. **44**, 348 (1953).

[2] O. Hashimoto, H. Tamura, Prog. in Part. and Nucl. Phys. **57**, 564 (2006).

[3] H. Tamura, M. Ukai, T. O. Yamamoto, T. Koike, Nucl. Phys. A **881**, 310 (2012).

[4] M. Agnello et al. (The FINUDA Collaboration), Phys. Lett. B **622**, 35 (2005).

[5] T. R. Saito et al., Nucl. Phys. A **754**, 3c (2004).

[6] P. Achenbach et al. (A1 Collaboration), Int. J. Mod. Phys. E **19**, 2624 (2004).

[7] P. Bydžovský, A. Gal, J. Mareš, Lect. Notes Phys. **724** (2006).

[8] D. J. Prowse, Phys. Rev. Lett. **17**, 782 (1966).

[9] M. Danysz et al., Nucl. Phys. **49**, 121 (1963).

[10] S. Aoki et al., Prog. Theor. Phys. **85**, 87 (1991).

[11] S. Bart et al., Phys. Rev. Lett. **83**, 5238 (1999).

[12] P. Veselý, E. Hiyama, J. Hrtánková, J. Mareš, in print Nucl. Phys. A, doi:10.1016/j.nuclphysa.2016.05.013.

[13] A. Ekström, et al., Phys. Rev. Lett. **110**, 192502 (2013).

[14] R. Machleidt, Phys. Rev. C **63**, 024001 (2001).

[15] M. Isaka, K. Fukukawa, M. Kimura, E. Hiyama, H. Sagawa, Y. Yamamoto, Phys. Rev. C **89**, 024310 (2014).

[16] Y. Yamamoto, T. Motoba, T. A. Rijken, Prog. Theor. Phys. Supp. **185**, 72 (2010).

[17] H. Hergert, P. Papakonstantinou, R. Roth, Phys. Rev. C **83**, 064317 (2011).

[18] L. D. Fadeev, Zh. Eksp. Theor. Fis. **39**, 1459 (1960).

[19] O. A. Yakubovsky, Sov. J. Nucl. Phys. **5**, 937 (1967).

[20] A. Nogga, Nucl. Phys. A **914**, 140 (2013).

[21] B. R. Barrett, P. Navrátil, J. P. Vary, Prog. Part. Nucl. Phys. **69**, 131 (2013).

[22] R. Wirth, et. al., Phys. Rev. Lett. **113**, 192502 (2014).

[23] J. J. Dean, M. Hjorth-Jensen, Phys. Rev. C **69**, 054320 (2004).

[24] H. Feldmeier, Nucl. Phys. A **515**, 147 (1990).

[25] M. Schaefer, H. Feldmeier, J. Mareš, T. Neff, PoS Bormio 2015, 036 (2015).

[26] V. Somá, C. Barbieri, T. Duguet, Phys. Rev. C **87**, 011303 (2013).

[27] J. Carlson, Phys. Rev. C **36**, 2026 (1987).

[28] P. Ring, P. Schuck, *The Nuclear Many-Body Problem* (Springer-Verlag, N.Y. 1980).

[29] B.D. Serot, J.D. Walecka, Adv. Nucl. Phys. **16**, 1 (1986).

[30] J. Mareš, B. K. Jennings, Phys. Rev. C **49**, 2472 (1994).

[31] T.H.R. Skyrme, Nucl. Phys. **9**, 615 (1959).
D.Vautherin, D.M. Brink, Phys. Rev. C **5**, 626 (1972).

[32] H.-J. Schulze, E. Hiyama, Phys. Rev. C **90**, 047301 (2014).

[33] J. Decharge, D. Gogny, Phys. Rev. C **21**, 1568 (1980).

[34] D. Bianco, F. Knapp, N. Lo Iudice, P. Veselý, F. Andreozzi, G. De Gregorio, A. Porrino, J. Phys. G: Nucl. Part. Phys. **41**, 025109 (2014).

[35] G. C. Wick, Phys. Rev. **80**, 268-272 (1950).

[36] D. Bianco, F. Knapp, N. Lo Iudice, F. Andreozzi, A. Porrino, Phys. Rev. C **85**, 014313 (2012).

[37] Y. Akaishi, T. Harada, S. Shinmura, K. S. Myint, Phys. Rev. Lett. **84**, 3539 (2000).

[38] Y.K. Gambhir, P. Ring, A. Thimet, Ann. Phys **198**, 132 (1990).

[39] I. Angeli, At. Data Nucl. Data Tab. **87**, 185 (2004).

[40] M. Agnello et al., Phys. Lett. B **698**, 219 (2011).

[41] R. E. Chrien, Nucl. Phys. A **478**, 705c (1988).

[42] T. Hasegawa et al., Phys. Rev. C **53**, 1210 (1996).

[43] H. Polinder, J. Haidenbauer, U. - G. Meißner, Nucl. Phys. A **779**, 244 (2006).

[44] T. England, M. Hjorth-Jensen, G.R. Jansen, CENS, a Computational Environment for Nuclear Structure, in preparation, folk.uio.no/mhjensen/cp/software.html.

[45] R. Roth, P. Papakonstantinou, N. Paar, H. Hergert, T. Neff, H. Feldmeier, Phys. Rev C **73**, 044312 (2006).